Modelling of plutonium diffusion in (U,Pu)O_2±x mixed oxide

P. Chakraborty, C. Guéneau, A. Chartier

Modelling of plutonium diffusion in $(U,Pu)O_{2\pm x}$ mixed oxide

P. Chakraborty, C. Guéneau[1], A. Chartier*

ISAS – Service de la Corrosion et du Comportement des Matériaux dans leur Environnement (SCCME), CEA, Université Paris-Saclay, F-91191 Gif-sur-Yvette, France

Abstract

The modelling of the thermo-kinetic properties of uranium-plutonium mixed oxide (MOX) is of utmost importance for optimizing its synthesis and for predicting its behaviour in Fast Breeder Reactors. Despite the stakes and likely because of experimental issues, little or no experimental data are available for the entire MOX system. We circumvent here the difficulties by developing a mobility database for plutonium using the DICTRA code. A well-established model of MOX formalized within the Compound Energy Formalism ensures the thermodynamic description. Rationalisation of the mobility parameters combined with the use of both cBΩ model and the few experimental data lead to a full and comprehensive description of plutonium self-diffusion in MOX for any plutonium content, O/M ratio and temperature. Additionally, we show that the observed plateau of the self-diffusion as a function of the oxygen to metal ratio (O/M) is related to the constant Pu^{3+} fraction for very low O/M ratio. Moreover, the observed minimum close to O/M = 2 is found for the lowest mobility of Pu^{4+}.

Keywords: self-diffusion, plutonium, plutonia, mixed oxide fuel, DICTRA

* Email address: christine.gueneau@cea.fr

Preprint submitted to Solid State Ionics

1. Introduction

Closing the fuel cycle in nuclear power plants has led nuclear industry to apply different strategies, depending on the technologies employed. In Light Water Reactors (LWRs) originally designed [1] to be loaded with uranium dioxide (UO_2) only, it was decided few decades ago to introduce plutonium in the form of uranium and plutonium mixed oxide (MOX). However, only MOX with low amount of plutonium can be loaded with moderate efficiency related to the thermal neutrons technology. In fast neutrons reactors, like sodium-cooled Fast Reactors (SFRs) for instance [2,3], burning of plutonium and minor actinides is ensured much more efficiently. The use of the nuclear fuel is therefore significantly improved and more importantly a much higher proportion of plutonium can be loaded [4] compared to LWRs.

For both thermal and fast neutrons reactors, one of the prerequisite of using MOX as a fuel is its sintering with appropriate properties. MOX has to be produced – safely – with controlled composition, stoichiometry, and microstructure and with a good homogeneity. For that purpose, and to optimize the process, one has to know in details the thermo-kinetic behaviour of the entire $UO_{2\pm x}$-PuO_{2-x} system. In addition, this knowledge is of outmost importance for the control of the homogeneity of fresh MOX fuel. This can avoid plutonium segregation, which has detrimental impact on the response of MOX fuel in pile, by decreasing locally its thermal conductivity [5].

The microstructure of MOX evolves very quickly in the early stage of its in-pile life in fast neutrons reactors [6]. The formation of a central void in the pellets in conjunction with the redistribution of plutonium, uranium and oxygen along their radius is observed. Plutonium tends to migrate towards the centre, increasing heat generation in this region. These behaviours – central void and redistribution of U / Pu– are commonly attributed to the effect of the high temperature gradient from the centre to the rim of the pellets [6]. It involves a coupling between mass flux transfer and temperature gradient, known as thermo-diffusion, whose understanding and prediction call – again – for precise knowledge of the thermo-kinetic properties of the $UO_{2\pm x}$-PuO_{2-x} system.

Indeed many experimental and theoretical studies have addressed physical and thermodynamic properties of the U-Pu-O ternary system [1,5,6,7,8,9]. It led to a reliable thermodynamic description with the CALPHAD model [10] that describes the $UO_{2\pm x}$ – PuO_{2-x} domain, i.e. for MOX. Conversely, mass transport is by far less documented. Recent works [9] have gathered and rationalized oxygen transport in MOX by means of DICTRA modelling [11]. Still, a comprehensive description and an applicable model for cation transport is missing. This is not surprising since – as we will see below – few measurements are available, particularly for MOX compositions enriched in plutonium.

The aim of the present work is to build a model for the transport of plutonium in MOX. The model and the approach followed herein is in line with previous works on oxygen transport [9,12]. We use a diffusion model as implemented in DICTRA, which is coupled to the well-established thermodynamic description of MOX in the $UO_{2\pm x}$ – PuO_{2-x} domain [10]. This diffusion model contains mobility parameters that were fitted in order to assess a complete and coherent description of plutonium diffusion in the above-mentioned mixed oxide at any temperature and oxygen partial pressure. To do so, we performed a careful selection of experimental data, and extended as far as possible by data obtained with the help of the so-called cBΩ model [13,14] for plutonia.

2. Modelling

2.1 Thermodynamic description of (U,Pu)$O_{2\pm x}$

The thermodynamic model of the U-Pu-O ternary system has mainly been established and described in a previous paper [10]. Marginal modifications were done few years later [11] to develop the oxygen mobility database. We recall only – for sake of utility – the description of the uranium-plutonium mixed oxide (MOX) and nearby domains of the phase diagram, where the crystal structure is maintained as fluorite.

The thermodynamic description of the Gibbs energy for MOX is formalized in the framework of the Compound Energy Formalism (CEF). Such a formalism states that each crystallographic lattice is represented by one specific sublattice as follows: (U^{3+}, U^{4+}, U^{5+}, Pu^{3+}, Pu^{4+}, Pu^{5+})$_1$ (O^{2-}, Va)$_2$ (O^{2-}, Va)$_1$. The first sublattice represents the fcc crystallographic site for cations and contains uranium or plutonium with different oxidation states, respectively U^{3+}, U^{4+}, U^{5+} and Pu^{3+}, Pu^{4+}, Pu^{5+}. The second sublattice (denoted ‘) stands for regular oxygen in its tetrahedral crystallographic site. The third and last sublattice (denoted ‘’) sets for oxygen interstitials. Both second and third sublattices can be filled by oxygen (O^{2-}) or can be empty (with Va: vacancy). Each possible combination of the above sublattices with a single species in each sub-lattice is called an end-member. The end-members may represent real compounds, like for example (U^{4+})$_1$(O^{2-})$_2$(Va)$_1$ for stoichiometric UO_2 or (Pu^{4+})$_1$(O^{2-})$_2$(Va)$_1$ for stoichiometric PuO_2. They may also have no connection to any real compound, and are then meant to describe deviations from stoichiometry. For example, (Pu^{3+})$_1$(Va)$_2$(Va)$_1$ is one of the end-member used for the description of hypo stoichiometric plutonia PuO_{2-x}. The combinations of some of the end-members correspond to fully reduced and fully oxidized key compositions like (U^{3+})$_1$($O^{2-}_{0.75}$Va$_{0.25}$)$_2$(Va)$_1$ for $UO_{1.5}$, (Pu^{3+})$_1$($O^{2-}_{0.75}$Va$_{0.25}$)$_2$(Va)$_1$ for $PuO_{1.5}$ and (U^{5+})$_1$(O^{2-})$_2$($O^{2-}_{0.5}$Va$_{0.5}$)$_1$ for $UO_{2.5}$ which are neutral and define the boundaries of the $UO_{2\pm x}$-PuO_{2-x} domain.

Within this CEF framework, a wide range of defect population can be described for the entire $UO_{2\pm x}$ – PuO_{2-x} region [10,11], as a function of composition, temperature or oxygen partial pressure. As an example, we report on Figure 1 the fraction of populations obtained using the model [11] and the Thermo-Calc software [15] for ($U_{0.75}Pu_{0.25}$)$O_{2\pm x}$, ($U_{0.5}Pu_{0.5}$)$O_{2\pm x}$ and ($U_{0.25}Pu_{0.75}$)$O_{2\pm x}$ at 1773 K. We observe in all examples that most populations drastically vary with the oxygen to metal ratio O/(U+Pu).

We start our description for ($U_{0.5}Pu_{0.5}$)$O_{2\pm x}$ from low hypo stoichiometry upward. In the range of O/(U+Pu) (O/M) ratio between 1.75 and roughly 1.87, hypo stoichiometry is carried by the second sub lattice (oxygen regular site (O^{2-})’) with vacancy fraction (Va)’ in the range of $1.3.10^{-1}$ – 6.10^{-2}. Cation fractions compensate the total charge with roughly twice the amount of plutonium in 3+ state Pu^{3+} in addition to the regular 4+ state Pu^{4+}. Uranium in its regular 4+ state U^{4+} remains at high values, and therefore does not participate much. For very low O/M ratio below 1.75, once plutonium is fully reduced into Pu^{3+}, uranium in 4+ state U^{4+} starts to be reduced into U^{3+}.

In the region from 1.87 up to exact stoichiometry 2, the accommodation of hypo stoichiometry becomes significantly more complex. The oxygen vacancy decreases along with plutonium in its 3+ state Pu^{3+}, and in the meantime uranium in 5+ state U^{5+} smoothly increases together with Pu^{4+} when getting closer to the exact stoichiometry.

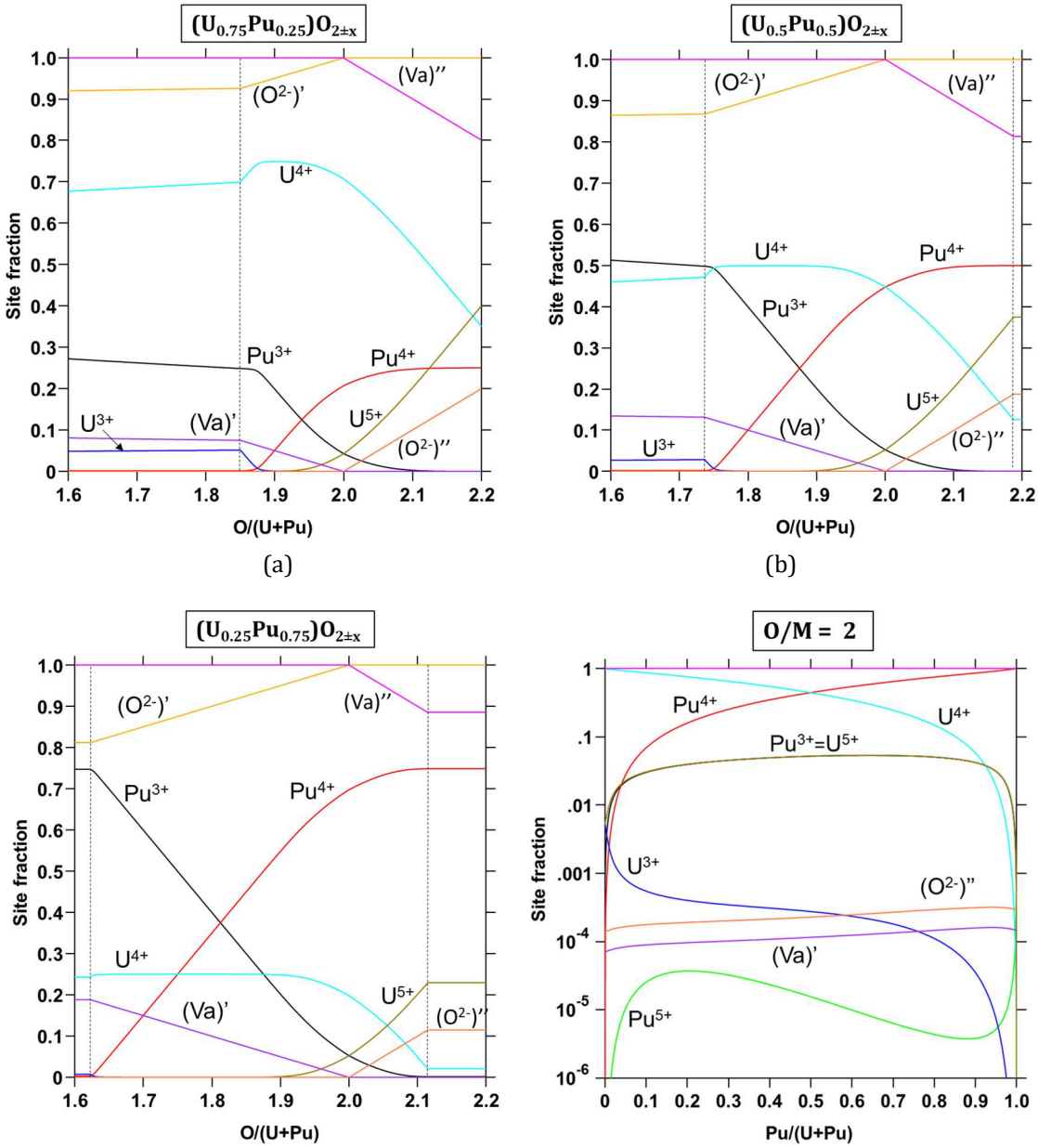

Figure 1: Calculated site fraction of the species at 1773 K in (a) $(U_{0.75}Pu_{0.25})O_{2\pm x}$, (b) $(U_{0.5}Pu_{0.5})O_{2\pm x}$ and (c) $(U_{0.25}Pu_{0.75})O_{2\pm x}$ as a function of O/M ratio (d) for a fixed O/M ratio equal to 2 as a function of Pu/(U+Pu) ratio, using the model [11]. The dashed lines indicate the phase boundaries.

At stoichiometry, oxygen interstitial and vacancy show equal concentration, compensating each other. The same is true for the population of U^{5+} and Pu^{3+} whose values are equal and much higher than oxygen defects in comparison, in line with what was noticed before for a lower amount of plutonium [9].

In the hyper stoichiometric region and starting from O/(U+Pu) ratio of 2.0, the accommodation of oxygen interstitial is carried by uranium in its 5+ state U^{5+}, with twice the amount. The rest of uranium and plutonium are in their regular 4+ state, U^{4+} and Pu^{4+}. Plutonium exhibits only one single valence state in this hyper stoichiometric region.

The trend as a function of the oxygen stoichiometry is the same for the other Pu contents (Figure 1 (a) and (c)). The main species are: U^{4+}, Pu^{3+}/Pu^{4+}, oxygen vacancies for O/M<2 and U^{4+}/U^{5+}, Pu^{4+} and oxygen interstitials for O/M>2. As expected, the mixed oxide is stabilized at hyper stoichiometric oxygen content by oxidation of uranium into U^{5+} for high U contents. On the other hand, the dioxide is more and more stabilized in the hypo stoichiometric range with increasing high Pu contents with the reduction of plutonium into Pu^{3+}. This can be explained by the difference in the oxygen potential between both $UO_{2\pm x}$ and PuO_{2-x} dioxides [8].

The fraction of populations are calculated at 1773 K as a function of Pu/(U+Pu) ratio at the exact oxygen stoichiometry 2 (Figure 1(d)). As expected, the fractions of the major cations Pu^{4+} and U^{4+} increase and decrease, respectively, with the plutonium content. The concentrations of Pu^{3+} and U^{5+} are equal to maintain the charge neutrality. The oxygen defects (vacancy and interstitial = oxygen Frenkel pair) do not vary much with the Pu content. Finally, the Pu^{5+} concentration remains very low in the entire system.

2.2 DICTRA model for plutonium self-diffusion

The description of plutonium diffusion in $(U,Pu)O_{2\pm x}$ is built following works performed earlier on iron oxides [16]. Herein, we start by considering the plutonium diffusion in the MOX along the z-direction. We may write the flux of plutonium J_{Pu} as function of the gradient of plutonium chemical potential μ_{Pu} as follows:

$$J_{Pu} = -D^{*}_{Pu}\frac{C_{Pu}}{RT}\frac{\partial \mu_{Pu}}{\partial z} \quad (1)$$

R and T are respectively the universal gas constant and the temperature in this equation, and C_{Pu} sets for the concentration of plutonium while D^{*}_{Pu} represents the self-diffusion coefficient. The self-diffusion coefficient can in turn be expressed as a function of the activation energy G_{act} and the mobility prefactor M^{0}_{Pu} for plutonium:

$$D^{*}_{Pu} = D^{0}_{Pu}exp\left(\frac{-G_{act}}{RT}\right) = M^{0}_{Pu}RTexp\left(\frac{-G_{act}}{RT}\right) = M_{Pu}RT \quad (2)$$

Due to its very low fraction whatever the MOX composition, as mentioned above, the mobility of Pu^{5+} will be neglected. Then, within the framework of the compound energy formalism CEF presented above, the contribution of the mobility parameter of plutonium M_{Pu} can be further separated into two terms, so that:

$$M_{Pu} = \frac{y_{Pu^{3+}} \times M_{Pu^{3+}} + y_{Pu^{4+}} \times M_{Pu^{4+}}}{y_{Pu^{3+}} + y_{Pu^{4+}}} \quad (3)$$

Each term, $M_{Pu^{3+}}$ and $M_{Pu^{4+}}$ is expressed by:

$$M_{Pu^{v+}} = M^{0}_{Pu^{v+}}RTexp\left(\frac{-G^{Pu^{v+}}_{act}}{RT}\right) \quad (4)$$

where v is the charge of plutonium cation.

In the mobility term for each cation, the activation energy $G_{act}^{Pu^{v+}}$ and prefactor $M_{Pu^{v+}}^{0}$ are subsequently decomposed as a function of all possible end-members that arise from the CEF, i.e. all possible combinations of occupation of all three sublattices. To be even more specific, this decomposition includes all possible charge states of uranium and all possible charge states of plutonium with empty or filled regular and interstitial oxygen sites:

$$RTln\, M_{Pu^{v+}}^{0} = \sum_{i=Pu^{3+},Pu^{4+},U^{3+},U^{4+},U^{5+}} y_i \times \sum_{j=O^{2-},Va} y_j \times \sum_{k=O^{2-},Va} y_k \times RTln\, M_{Pu^{v+}}^{0\,(i)(j)(k)} \quad (5)$$

$$G_{act}^{Pu^{v+}} = \sum_{i=Pu^{3+},Pu^{4+},U^{3+},U^{4+},U^{5+}} y_i \times \sum_{j=O^{2-},Va} y_j \times \sum_{k=O^{2-},Va} y_k \times G_{Pu^{v+}}^{(i)(j)(k)} \quad (6)$$

Obviously, parameters are numerous. For sake of simplicity, we present the example of pure plutonia, for which the sublattice model reduces then as follows: $(Pu^{3+}, Pu^{4+})_1$ $(O^{2-}, Va)_2$ $(O^{-2}, Va)_1$. For each charge of plutonium, there are 4 end-members. For Pu^{4+} for instance, the end-members are $(Pu^{4+})_1(O^{2-})_2(O^{2-})_1$; $(Pu^{4+})_1(O^{2-})_2(Va)_1$; $(Pu^{4+})_1(Va)_2(O^{2-})_1$ and $(Pu^{4+})_1(Va)_2(Va)_1$. We will write it more synthetically in the form of $(Pu^{4+})_1(*)_2(*)_1$, with * being O^{2-} or Va. We have therefore eight endmembers from which each mobility term can be decomposed. Hence, the mobility term of Pu^{4+} (in plutonia) depends upon all possible mobility terms $M_{Pu^{4+}}^{(i)(j)(k)}$ associated to each end-member, and to their fractions y_i, y_j and y_k with i $\in$ (Pu^{3+}, Pu^{4+}) and j, k $\in$ (O^{2-},Va).

For MOX, the number of parameters for plutonium diffusion – i.e. mobilities associated to each of the end-members – and their activation energies increases up to 40 each, and therefore the total number of parameters is 80. These 80 parameters have to be fitted carefully for a reliable description of the diffusion. However, a so high number of parameters may weaken the robustness of the fitting. Additionally, some of these parameters have no straightforward physical meaning. We therefore made some choices in order to drastically reduce the total number of parameters.

We assume that mobilities and activation energies of Pu^{3+} and Pu^{4+} are related to the content of the cation sublattice (plutonium or uranium), whatever the content of the oxygen sublattices. However, it has to be noted that the influence of the oxygen stoichiometry is described through the site fractions of oxygen defects (interstitials and vacancies) from the thermodynamic model (see equations 5 and 6), as reported by Matthews et al [17] in their atomistic calculations. In other words, the oxygen mobility being much higher compared to plutonium [9], it is considered as uncorrelated to plutonium and therefore should have only marginal influence on its mobility. Hence, each end-member $(U^{3+})_1(*)_2(*)_1$, $(U^{4+})_1(*)_2(*)_1$, $(U^{5+})_1(*)_2(*)_1$, $(Pu^{3+})_1(*)_2(*)_1$ and $(Pu^{4+})_1(*)_2(*)_1$ bears only one mobility prefactor and one activation energy for each charge state of each cation. Within these assumptions, the number of parameters reduces down to 10 mobility prefactors and to 10 activation energies, which is much more tractable and hopefully more reliable.

By setting additional relationships between the mobility parameters in equations 7, 8, 9 and 10, we were able to simplify even more the model and to decrease the number of mobility parameters down to 6 mobility prefactors and 6 activation energies. The parameters for Pu^{3+} or Pu^{4+} in PuO_2 whatever the charge of Pu is, in the cation sublattice, were taken equal due to the lack of data for Pu diffusion in PuO_2. Thus, we set for Pu diffusion in PuO_2:

$$M_{Pu^{3+}}^{(Pu^{3+})(*)(*)} = M_{Pu^{3+}}^{(Pu^{4+})(*)(*)} = M_{Pu^{3+}}^{(Pu^{5+})(*)(*)} \quad (7)$$

$$M_{Pu^{4+}}^{(Pu^{3+})(*)(*)} = M_{Pu^{4+}}^{(Pu^{4+})(*)(*)} = M_{Pu^{4+}}^{(Pu^{5+})(*)(*)} \quad (8)$$

As mentioned in section 2.1, for low O/M ratio, Pu^{3+} is the major Pu cation whereas Pu^{4+} is predominant for O/M≥2. The mobilities of Pu^{3+} (or Pu^{4+}) have been taken equal in UO_2 containing either U^{3+} or U^{4+}, corresponding to a MOX with a low O/M ratio. This will be necessary to represent the plateau observed for low O/M values (<1.9) as we will see in the following. So, we set for Pu diffusion in UO_2:

$$M_{Pu^{3+}}^{(U^{3+})(*)(*)} = M_{Pu^{3+}}^{(U^{4+})(*)(*)} \quad (9)$$

$$M_{Pu^{4+}}^{(U^{3+})(*)(*)} = M_{Pu^{4+}}^{(U^{4+})(*)(*)} \quad (10)$$

The mobility term for Pu^{4+} diffusion in UO_2 that is $M_{Pu^{4+}}^{(U^{5+})(*)(*)}$, captures the trends of diffusion for O/M>2 where U^{5+} is stable. Finally the mobility of Pu^{3+} in UO_2 containing U^{5+}, $M_{Pu^{3+}}^{(U^{5+})(*)(*)}$, takes low values to reach the minimum at the O/M ratio closed to 2, where these species (Pu^{3+} and U^{5+}) are stable with low concentrations (see Figure 1).

In addition to these mobility parameters, it has been necessary to introduce an interaction parameter $G_{(Pu^{4+},U^{4+})}$ between (Pu^{4+},U^{4+}) to add a plutonium composition dependent term in order to obtain a good agreement with the experimental data for O/M=2. The introduction of this interaction parameter modifies the mobility of Pu^{4+} in UO_2 containing U^{4+} as follows:

$$M_{Pu^{4+}}^{(U^{4+})(*)(*)} = y_{U^{4+}} \times M_{Pu^{4+}}^{0\,(U^{4+})(*)(*)} \times RTexp\left(\frac{-G_{Pu^{4+}}^{(U^{4+})(*)(*)} + y_{Pu^{4+}} y_{U^{4+}} G_{(Pu^{4+},U^{4+})}}{RT}\right) \quad (11)$$

Finally, in this approach, the self-diffusion of plutonium is modelled by the mobilities of Pu^{3+} and Pu^{4+} and considering different charge states for uranium (U^{3+}, U^{4+} or U^{5+}) to represent the change in the O/M ratio of the MOX.

Overall, 13 parameters have to be fitted against reliable data that are presented below. Experimental measurements available in literature are reviewed and carefully selected. It is completed with semi-empirical data provided by the cBΩ model.

3. Data for the mobility database development

3.1 Experimental data for Pu self-diffusion in (U,Pu)$O_{2\pm x}$

We report the references of all the available experimental data for plutonium self-diffusion in PuO_2 and $(U,Pu)O_{2\pm x}$ in Table 1 in chronological order. Before any detailed discussion, it is worth mentioning that the available data are scarce (eight studies only) and split. Thus, we observe that (i) among the eight studies only three of them have been made on single crystals, (ii) no data are available for plutonium content above 45% and (iii) most temperatures of investigation are above 1700 K.

First sets data on $(U,Pu)O_2$ were acquired in the sixties – seventies by Lindner *et al* [18], Riemer and Scherff [19], Matzke [20] and Schmitz and Marajowsky [21] using plutonium tracer diffusion on polycrystals. From the analysis of their data, Lindner *et al* [18] reported an activation energy for diffusion quite low compared to pure UO_2. The authors explained that it could be due to a small positive deviation from the stoichiometry. Later Matzke [20] along with Schmitz and Marajowsky [21] investigated hypo stoichiometric oxygen compositions and reported the existence of a minimum at an O/M slightly below 2. The disturbing surface phenomena (polishing damage, high temperature surface relaxation, mass transfer by evaporation-condensation) have been widely discussed in details by both Lambert [22] and Matzke [23] a decade later. They suggested that careful conditions might help to measure reliable data.

Compounds	O/M	T (K)		Authors
$(U_{0.85}Pu_{0.15})O_{2+x}$	2.00017± 0.001	1173 - 1873	Polycrystals	Lindner et al 1967 [18]
$(U_{0.85}Pu_{0.15})O_{2+x}$	2.05 - 2.12	1473 - 1773	Polycrystals	Riemer et al 1971 [19]
$(U_{0.85}Pu_{0.15})O_{2-x}$	-	1773 - 1873	Polycrystals	Matzke 1973 [20]
$(U,Pu)O_{2-x}$	< 2 (4,10,15,20,30 Pu)*	1783	Polycrystals	Schmitz et al 1975 [21]
UO_2	~2*	1783	Single crystals	Schmitz et al 1975 [21]
UO_2	2.000 ± 0.002	1873 - 2173	Single crystals	Lambert 1978 [22]
$(U_{0.8}Pu_{0.2})O_{2\pm x}$	1.9 - 2.15	1773 - 1973	Single crystals	
$(U_{0.82}Pu_{0.18})O_{2\pm x}$	-*	1773 - 1973	Single crystals	Matzke 1983 [23]
$(U_{0.55}Pu_{0.45})O_{2-x}$	1.95 - 1.98	1745 - 1970	Polycrystals	Noyau 2012 [24]

*O/M ratio not given in the original paper

Table 1: Plutonium tracer diffusion data in $(U,Pu)O_{2\pm x}$

In 1978, for the first time, a meticulous experimental work was performed on single crystals of both UO_2 and $(U_{0.8}Pu_{0.2})O_{2\pm x}$ by Lambert in his thesis [22]. The author found lower values for diffusion than the previous published data. He used single crystals instead of poly-crystals and better controlled experimental conditions. A diffusion minimum was also observed at O/M = 1.98 which was explained by a change in the diffusion mechanism: interstitial and vacancy mechanisms at lower and at higher O/M ratio, respectively. The position of the minimum was found to change with the temperature in a similar manner as already observed in magnetite $Fe_{3-x}O_4$ [16]. Measurements by Matzke on $(U_{0.82}Pu_{0.18})O_{2\pm x}$ single crystals confirmed a minimum at O/M=1.98 and a similar shape of the data as for $(U_{0.80}Pu_{0.20})O_{2\pm x}$ [23].

No new measurements were achieved for a long time. Only recently, S. Noyau [24] performed plutonium tracer diffusion measurements using SIMS on $(U_{0.55}Pu_{0.45})O_{2-x}$ polycrystals. The contribution of the grain

boundaries was estimated. The obtained volume diffusion coefficients are lower than the findings of Lambert [22] for UO_2 and 18 % Pu and also of Matzke [23] for 20 % Pu.

For the modelling with DICTRA, we selected the experimental data of Riemer and Scherff [19] on $(U_{0.85}Pu_{0.15})O_{2+x}$, Lambert [22] on UO_2 and $(U_{0.8}Pu_{0.2})O_{2\pm x}$, Matzke [23] on $(U_{0.82}Pu_{0.18})O_{2\pm x}$ and Noyau [24] on $(U_{0.55}Pu_{0.45})O_{2-x}$. The data of Lindner et al [18] were discarded due to the very low activation energy, in disagreement with all other measurements. The data of Schmitz and Marajofsky [21] were not selected due to their higher values compared to Lambert [22] and Matzke [23] probably due to the use of polycrystalline samples. In case the O/M ratio was not given by the authors [23], it was calculated from the oxygen partial pressure using the thermodynamic model used in this work [10,24].

No experimental data exists on Pu self-diffusion coefficient in PuO_2. Kutty *et al* [25] deduced activation energy data for Pu^{3+} and Pu^{4+} in PuO_2 from indirect experimental work on sintering. Very recently Wang *et al* [26] calculated migration energy of Pu vacancy and interstitial in PuO_2 using Molecular Dynamics simulations. Theoretical methods were also used to determine activation energies for plutonium self-diffusion on stoichiometric $(U_{0.75}Pu_{0.25})O_2$ by using DFT+U electronic structure calculations [27]. The lack of data has motivated the use of the cBΩ model to provide additional input data for the modelling with DICTRA.

3.2 cBΩ model for Pu self-diffusion in $(U,Pu)O_{2\pm x}$

The 'cBΩ model' was promoted some years ago by Varotsos and Alexopoulos [13,14] in order to predict diffusion coefficients – as long as a single mechanism for diffusion is involved – in large domains of temperature (and pressure) with only few measurements. In this model, the activation energy is linearly dependent upon the Bulk Modulus (B) and the mean volume per atom (Ω). Hence, self-diffusion D as a function of temperature T reads as:

$$D = f a^2 \nu \exp\left(-\frac{cB\Omega}{k_B T}\right) \qquad (12)$$

The pre-factor is composed by the correlation factor f, the characteristic length for diffusion a and the attempt frequency ν. The parameter c that appears in the activation energy is the parameter to be fitted for each compound considered.

We apply the cBΩ model for cation diffusion in oxides, at stoichiometry 2 and with fluorite structures. It includes cation self-diffusion in ThO_2 and oxygen self-diffusion in Li_2O, in addition to the one of UO_2. We did not consider fluoride compounds like SrF_2 or CaF_2, despite abundant measurements. They exhibit much more ionic bonds compared to oxides and their behavior might depart from them. We subsequently extrapolated the model for plutonia by applying a linear law to the parameter c with respect to the ionic radii of diffusing species.

In AB_2 fluorite compounds, it is known that diffusion of "A" species operates throughout a vacancy mechanism [28]. We therefore choose to set the correlation factor in the Equation 12 as being f = 0.78149 for

vacancy diffusion in fcc crystal [29]. The attempt frequencies are fixed to the Debye frequencies of each compounds. They come from references cited by Eser et al [30] for UO_2, ThO_2 and PuO_2 and from Hull et al for Li_2O [31]. They are reported in Table 2. Cell parameters are used as the characteristic length for diffusion. We set the values to the ones extrapolated down to 0 K, quoted here as a_0. We got values from Fink [32] for Urania, from Yamashita *et al* [33] for thoria and plutonia, and from Hull *et al* [31] for lithia.

Apart from the fitting parameter c, the activation energies involve the Bulk modulus and the formation volume of the diffusing defect. Following Varotsos [13], we set formation volumes to mean volumes per atom Ω. This mean volumes can be calculated from the cell parameters (a_0 mentioned above). We choose to write it as $\Omega = a_0^3/4$ since fluorite structure has 4 cations per conventional cell. A different choice could have been done – like $\Omega = a_0^3/12$. However, it would have changed the value of c, but not its relative evolution in the fluorite family. Bulk modulus are set to their values extrapolated at 0 K and are reported in Table 2. We extrapolated values from Idiri *et al* [34] for urania, thoria and plutonia, and from Hull *et al* [31] for lithia.

Compounds	PuO_2	UO_2	ThO_2	Li_2O
ν_D (THz)	54.4 [30]	49.3 [30]	51.4 [30]	141.5 [31]
$\mathbf{a_0^2}$ (T = 0K) (Å^2)	28.96 [33]	29.73 [32]	31.18 [33]	20.91 [31]
B_0 (T = 0K) (GPa)	191.0 [34]	215.4 [34]	207.5 [34]	84.5 [31]
Ω_0 (T = 0K) (Å^3)	38.96 [33]	40.52	43.52 [33]	23.90 [31]
c	0.0859	0.0982	0.1094	0.2131
Ionic radius (Å)	0.96	1.00	1.05	1.42

Table 2: Parameters used for PuO_2, UO_2, ThO_2 and Li_2O for the cBΩ model. Values of c for UO_2, ThO_2 and Li_2O are obtained from fitting to the experimental data as shown in Figure 2. The value c for PuO_2 is extrapolated from its linear evolution as a function of ionic radius of cations for UO_2 and ThO_2 and oxygen for Li_2O as reported on Figure 3.

Values of c in the equation 12 have been fitted against experimental data for UO_2, ThO_2 and Li_2O using a simple minimisation procedure implemented in a python code. They are reported in Table 2 and the fittings against experimental data can be visualized on Figure 2. Although not perfect for UO_2, the cBΩ model nevertheless captures the main trends for all three oxides considered.

Having values of c for three oxides, namely UO_2, ThO_2 and Li_2O, we extrapolate its value for plutonium in plutonia as shown in Figure 3. We consider for that purpose that the c value obeys a linear law with the ionic radius of the diffusing cation for urania and thoria and oxygen for lithia or "A" species in AB_2 fluorite structures. Such consideration follows previous findings obtained decades ago on diffusion in fluorite [35]. The extrapolation gives a value of c = 0.0859 reported in Table 2 and on Figure 2.

Prefactors and activation energies for all compounds are reported in Table 3 and compared to the available experimental data for UO_2, ThO_2 and Li_2O. Calculated activation energies for UO_2 and ThO_2 are in good agreement with experimental data. Both prefactors are slightly underestimated by the cBΩ model. However, prefactors are very sensitive to the fitting and this might explain the difference. Conversely, both activation energy and prefactor are more poorly fitted for Li_2O. Obviously, not all data were taken into account to extract both of them by Ando et al [36]. A simple fit of the available data with the Arrhenius law gives a prefactor of 7.3 10^{-4} m^2/s, very different from the one reported by these authors.

Having in mind the limitations of the cBΩ model, we find a value of $D_0 = 1.2\ 10^{-5}$ m^2/s and $E_{act.} = 4.0$ eV for plutonium self-diffusion in PuO_2. This value is close to the 4.11 eV obtained by Kutty et al [25] for Pu^{3+} for hypo stoichiometric plutonia. At the exact stoichiometry, Kutty *et al* estimated the activation energy for Pu^{4+} diffusion to be much higher at 5.95 eV.

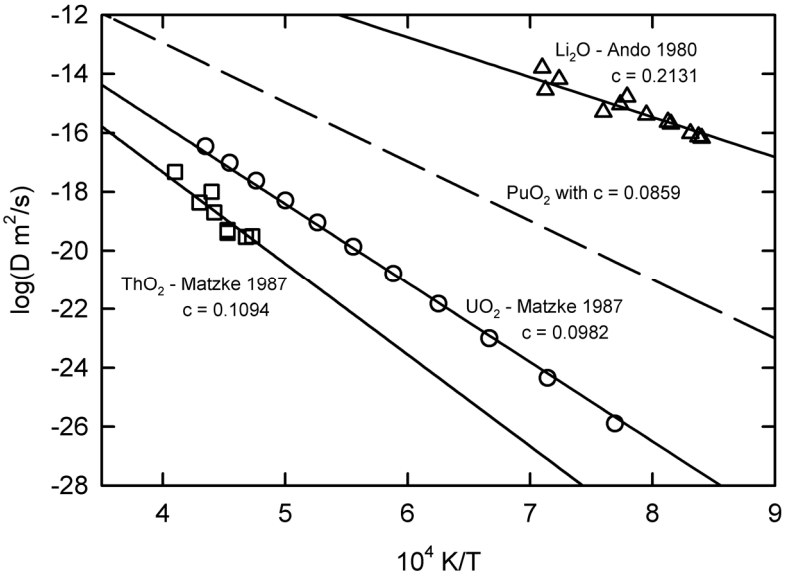

Figure 2: Self-diffusion of cation in fluorite structures PuO_2, UO_2, ThO_2 and self-diffusion of oxygen in anti-fluorite Li_2O. Symbols set for experimental data (open circles for UO_2 [37], open squares for ThO_2 [37], and open triangles for Li_2O [36]) and continuous lines are from cBΩ fitting of the experimental data (values of c are reported). Dashed line is for PuO_2; the value of c has been obtained using the extrapolation reported on Figure 3.

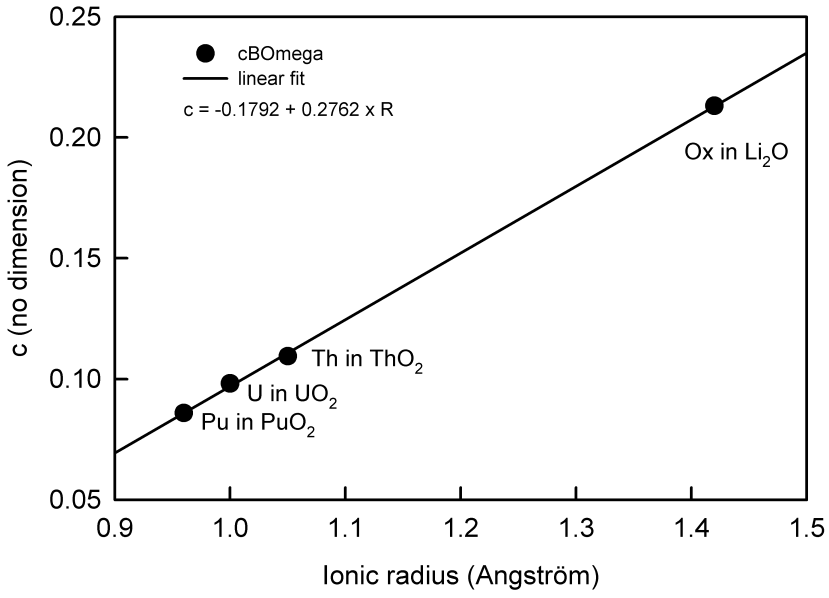

Figure 3: Evolution of the parameter c of the cBΩ model as a function of the ionic radius (quoted R in the equation) for cation self-diffusion in fluorites PuO_2, UO_2, ThO_2 and oxygen self-diffusion in anti-fluorite Li_2O. The value of c for PuO_2 has been extrapolated from the linear equation fitted on the other compounds.

Compounds	PuO_2	UO_2	ThO_2	Li_2O
D_0 (m^2/s)	$1.2\ 10^{-5}$	$1.2\ 10^{-5}$	$1.3\ 10^{-5}$	$2.3\ 10^{-5}$
exp.		$6.5\ 10^{-5}$ [37]	$3.5\ 10^{-5}$ [38]	$1.5\ 10^{-1}$ [36]
E_{act} (eV)	4.0	5.4	6.2	2.7
exp.	4.1 – 6.0 [25]	5.6 [37]	6.5 [37]	3.6 [36]
c	0.0859	0.0982	0.1094	0.2131
Ionic radius (Å)	0.96	1.00	1.05	1.42

Table 3: Calculated and experimental prefactors and activation energies for cation diffusion for PuO_2, UO_2, ThO_2 and oxygen diffusion for Li_2O. Ionic radii and c values of the cBΩ model are reported too.

4. Results

4.1 Assessment of the mobility parameters for Pu in MOX

In a first step, we assessed independently the plutonium mobilities for both PuO_2 and UO_2 endmembers. Thus, the plutonium self-diffusion data in PuO_2 from the cBΩ model were used to assess the Pu^{4+} mobility $M_{Pu^{4+}}^{(Pu^{4+})(*)(*)}$. For the Pu^{3+} diffusion in PuO_2, the activation energy for Pu^{3+} has been increased by a factor of 1.04 considering its larger ionic radius (1 Å) compared to Pu^{4+} (0.96 Å), following previous findings [35]. In parallel, the mobility parameters $M_{Pu^{4+}}^{(U^{4+})(*)(*)}$ for Pu^{4+} diffusion in UO_2 were assessed using the experimental data of Pu tracer diffusion in UO_2 [22]. As shown in Figure 4, very good agreements were obtained between calculated and experimental data for plutonium diffusion coefficient in both UO_2 and PuO_2.

Once these parameters fixed, the variation of the Pu diffusion coefficient with the oxygen stoichiometry was modelled by assessing the mobility parameters of Pu^{3+}, Pu^{4+} and Pu^{5+} with U^{3+} and U^{5+} in the cation sublattice. $M_{Pu^{3+}}^{(U^{3+})(*)(*)}$ was optimized for low O/M<2 for which it is the main contributor to the diffusion. $M_{Pu^{3+}}^{(U^{5+})(*)(*)}$ acts on the deep minimum close to 2 and was fitted accordingly. And $M_{Pu^{4+}}^{(U^{5+})(*)(*)}$ was adjusted to capture the faster diffusion observed experimentally for large O/M>2. For these fittings, the selected experimental data in section 3.1 were used. As mentioned in section 2.2, an interaction parameter was also introduced to achieve a final good agreement. The assessed mobility parameters of the DICTRA model are listed in Table 4.

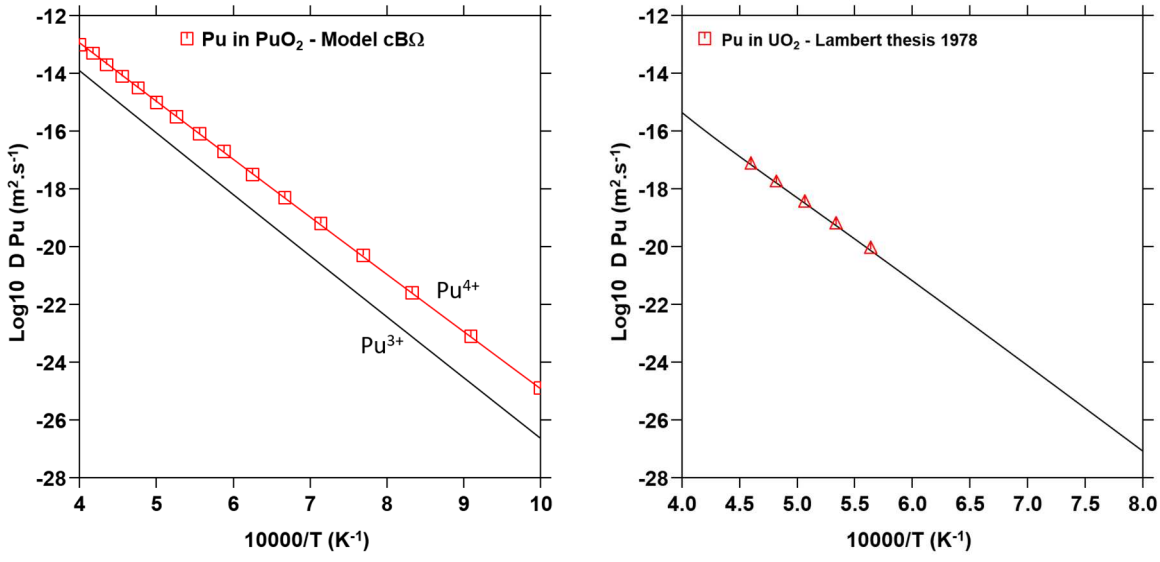

(a) (b)

Figure 4: Calculated Pu self-diffusion coefficient against reciprocal temperature (a) in PuO_2 compared to the cBΩ model (b) in UO_2 compared to experimental data of Lambert [22].

Compound	Diffusing Species	End-member	Prefactor ($m^2.s^{-1}$)	Activation energy (kJ/mol and eV)
PuO_2	Pu^{3+}	$(Pu^{3+})(*)(*)$	$1\ 10^{-10}$	393600 (4.1)
	Pu^{3+}	$(Pu^{4+})(*)(*)$	$1\ 10^{-10}$	393600 (4.1)
	Pu^{3+}	$(Pu^{5+})(*)(*)$	$1\ 10^{-10}$	393600 (4.1)
	Pu^{4+}	$(Pu^{3+})(*)(*)$	$3\ 10^{-10}$	370000 (3.85)
	Pu^{4+}	$(Pu^{4+})(*)(*)$	$3\ 10^{-10}$	370000 (3.85)
	Pu^{4+}	$(Pu^{5+})(*)(*)$	$3\ 10^{-10}$	370000 (3.85)
$(U,Pu)O_2$	Pu^{3+}	$(U^{3+})(*)(*)$	$2\ 10^{-8}$	560000 (5.8)
	Pu^{3+}	$(U^{4+})(*)(*)$	$2\ 10^{-8}$	560000 (5.8)
	Pu^{3+}	$(U^{5+})(*)(*)$	$1\ 10^{-20}$	1000000 (10.4)
	Pu^{4+}	$(U^{3+})(*)(*)$	$4\ 10^{-9}$	540000 (5.6)
	Pu^{4+}	$(U^{4+})(*)(*)$	$4\ 10^{-9}$	540000 (5.6)
	Pu^{4+}	$(U^{5+})(*)(*)$	$1\ 10^{-3}$	350000 (3.65)
$(U,Pu)O_2$	Pu^{4+}	$(Pu^{4+},U^{4+})(O^{2-})(Va)$		-450000

Table 4: Assessed mobility parameters for Pu selfdiffusion in $(U,Pu)O_{2\pm x}$. The line at the bottom of the table refers to the interaction parameter $G_{(Pu^{4+},U^{4+})}$ (see equation (11) in section 2.2).

4.2 Comparison with experimental data

We first focus on the evolution of the diffusion coefficient of Pu as a function of stoichiometry for MOX containing 15 and 18 % Pu (see Figure 5) and containing 20 and 45 % Pu (see Figure 6). In addition to the comparison of the total diffusion coefficient of Pu, we report on both figures the underlying fractions of defects as calculated from the thermodynamic model and the contribution of each Pu^{3+} and Pu^{4+} diffusion coefficients.

We observe that the overall shape of Pu diffusion coefficient against O/M ratio is well reproduced by our model for all compositions (see top of Figure 5 and top of Figure 6). We may divide the behaviour of the diffusion coefficient in three regions, according to the relative contributions of Pu^{3+} and Pu^{4+} species:

- For low O/M ratio below ~1.9 (1.93 for 15 Pu, 1.78 for 45 % Pu), the Pu diffusion coefficient reaches a plateau as suggested by Lambert [22] and Matzke [23], where the mobilities of Pu^{4+} and Pu^{3+} are constant with very close values. The existence of this plateau relies on the Pu^{3+} fraction that remains constant in this region, following the full reduction of Pu^{4+} into Pu^{3+}.
- For intermediate O/M ratio ranging between ~1.9 (1.93 for 15 Pu, 1.78 for 45 % Pu) and 2, the Pu diffusion coefficient decreases with the O/M ratio with Pu^{3+} being the major diffusing species. Pu diffusion exhibits a minimum value at a O/M ratio very close to 2 where the Pu^{4+} and Pu^{3+} mobilities are equal whereas Pu^{4+} diffusion coefficient is minimum at about O/M=1.98 (and 1.97 for 45 % Pu). The defect model can again explain this variation: in this region, Pu^{3+} is the major species whose fraction decreases up to a low value at O/M=2 whereas Pu^{4+} fraction increases.
- For O/M higher than 2, Pu diffusion coefficient increases with the O/M ratio with Pu^{4+} as major diffusing species consistently with the thermodynamic model.

While the calculated Pu diffusion coefficients show a reasonable agreement for most experimental data, considering the large uncertainties on these data, it significantly departs for hyper stoichiometric $(U_{0.85}Pu_{0.15})O_{2+x}$ for which the model underestimates the Pu diffusion coefficients compared to the experiments. As the calculated data for $(U_{0.8}Pu_{0.2})O_{2+x}$ are in a good agreement with the data of Matzke [23] and Lambert [22], a possible explanation could be that the experimental data for 15 and 20 % Pu are inconsistent with each other. New experiments in this composition range would be very useful to improve the modelling.

In addition, the minimum of the diffusion coefficient is calculated at O/M~2 instead of 1.98 with our model. The shift of the minimum towards lower O/M ratio with increasing temperature could not be reproduced too. This could be explained by the simplicity of our defect model in which no metal vacancy nor interstitial was considered. On the contrary, this peculiar behaviour was successfully accounted with DICTRA for iron oxides likely thanks to the modelling that includes iron vacancy and interstitial sites [16]. Thus, the introduction of vacancies in the cation sublattice might improve the present model.

We now turn to the Pu diffusion coefficient against Pu/(U+Pu) ratio as reported in Figure 7 and calculated at the exact stoichiometry at 1773 K. The diffusion coefficient exhibits a U-shape, with a minimum at around 30% of plutonium in MOX. Values of diffusion close to Urania are much lower than the ones close to Plutonia, by around four order of magnitudes. It origins from the high values obtained in PuO_2 with the cBΩ model. The experimental data are very scarce for comparison, and new experimental data would be useful to confirm these findings and to refine the model.

Finally, we report in Table 5 the calculated activation energies and pre factors for Pu self-diffusion in PuO_2, UO_2 and $(U,Pu)O_{2\pm x}$ along with the data coming from the literature.

As expected, the fitted activation energies are in good agreement with data from cBΩ model for PuO_2 and with experiments [22] for UO_2: they were both starting points of the fitting procedure. The pre factor of PuO_2 is well fitted too, while the one of UO_2 is slightly overestimated.

For intermediate compositions, the fitted values of activation energies and pre factors depart from experimental data. For $(U_{0.80}Pu_{0.20})O_{2\pm x}$, the activation energies are compared to the estimations based on a point defect model, with the hypothesized defects. The agreement is very good for $O/M < 2$ whereas the two activation energies for $O/M \geq 2$ are very different from the point defect data [23]. However, the model captures the increase of the activation energy at the exact stoichiometry. For $(U_{0.75}Pu_{0.25})O_2$, the fitted activation energies exhibit a factor two with the estimated data from DFT calculations [27]. Last the activation energy is much better reproduced for $(U_{0.55}Pu_{0.45})O_{2-x}$, but the pre factor is lower than the experimental value [24].

The agreement with the experimental data is mainly better for $O/M<2$. This could be explained by both possible inconsistencies between some of the data in the literature. Our model seems to be too simple for $O/M>2$ and likely deserves improvements by the introduction of metal vacancies and clusters of oxygen defects. Bearing in mind all limitations, a full thermokinetic model using DICTRA is now available for plutonium diffusion in MOX. This model reproduces reasonably well the scarce data coming from the literature. It can be used to calculate Pu and oxygen diffusion data for any O/M, Pu content and temperature in $(U,Pu)O_{2\pm x}$.

Calculated datasets for plutonium diffusion in $(U,Pu)O_{2\pm x}$ with Pu/(U+Pu)=0.1, 0.2, 0.3, 0.4, 0.5, 0.6, 0.7, 0.8, 0.9 as a function of the O/M ratio at 1273, 1773 K, 2273 K are given in supplementary materials. For information, a figure with a comparison of the calculations with the experimental data of Schmitz and

Marajofsky [21] is also reported. As expected the calculated diffusion coefficients are significantly lower than the experimental data.

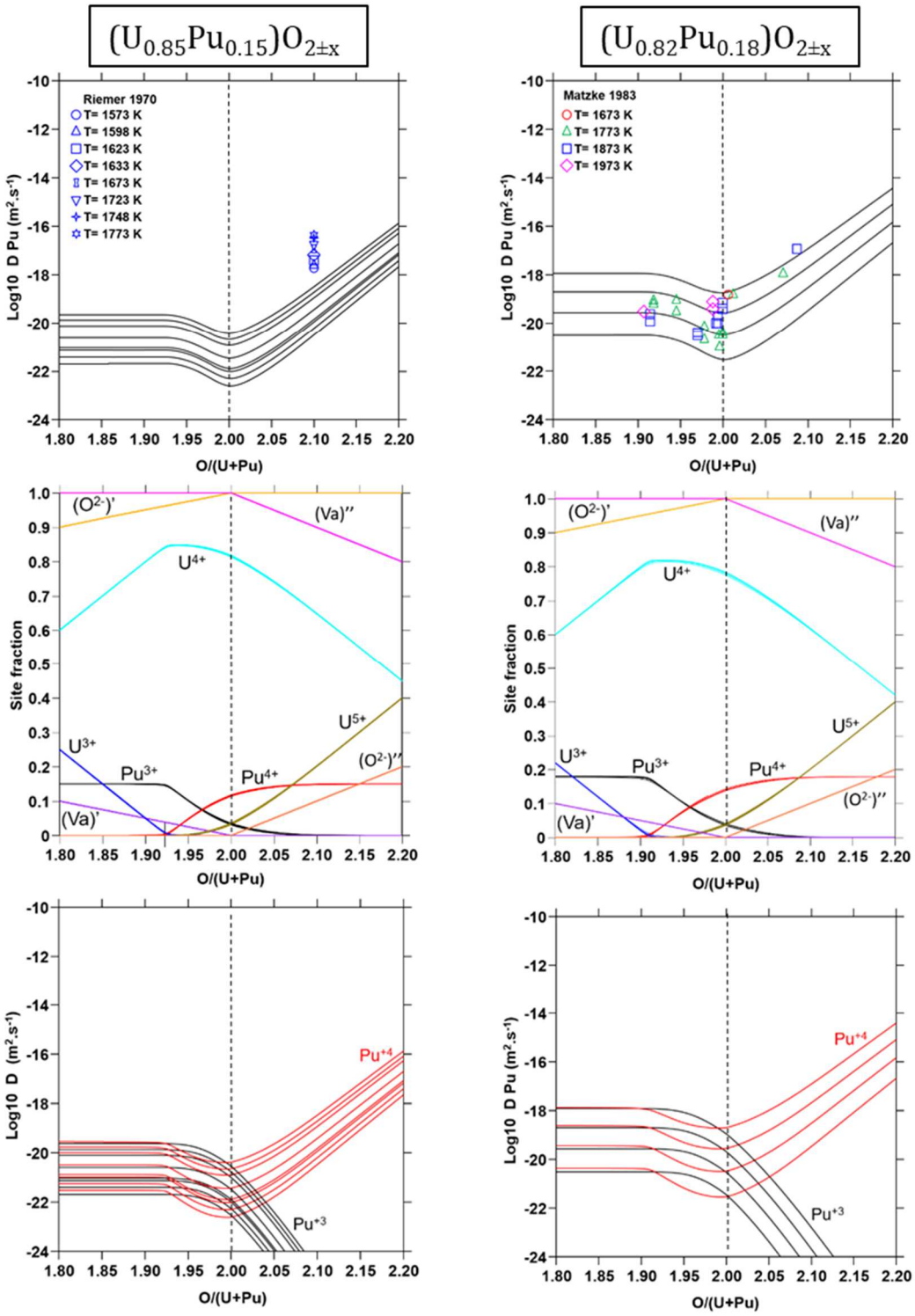

435 Figure 5: Calculated data for $(U_{0.85}Pu_{0.15})O_{2\pm x}$ (left) and $(U_{0.82}Pu_{0.18})O_{2\pm x}$ (right) versus O/M ratio: Pu diffusion coefficient (top), Species site fractions (middle), Pu^{3+} and Pu^{4+} diffusion coefficients (bottom). The experimental data of Riemer [19] and Matzke [23] are reported.

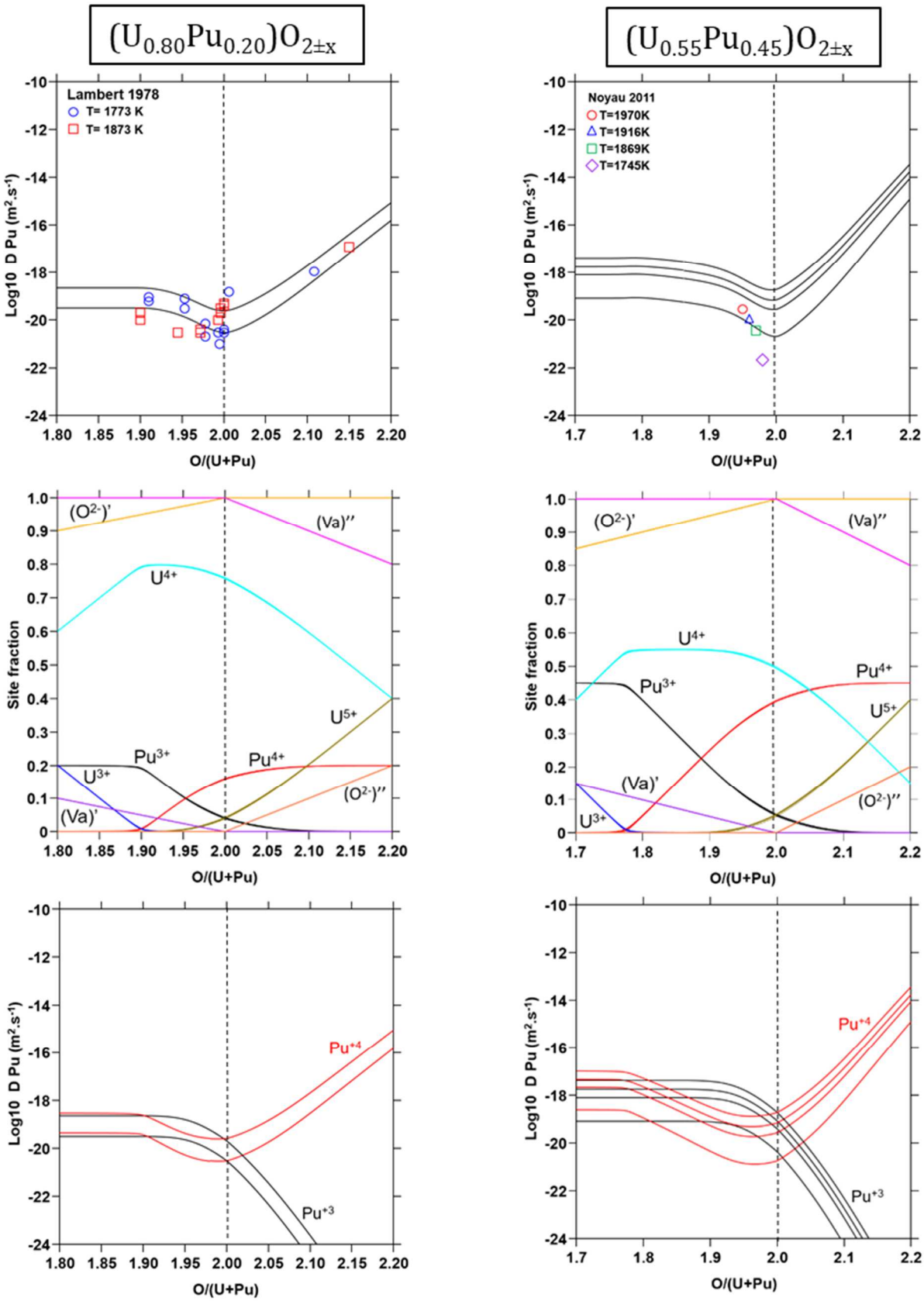

440 Figure 6: Calculated data for $(U_{0.80}Pu_{0.20})O_{2\pm x}$ (left) and $(U_{0.55}Pu_{0.45})O_{2\pm x}$ (right) versus O/M ratio: Pu diffusion coefficient (top), Species site fractions (middle), Pu^{3+} and Pu^{4+} diffusion coefficients (bottom). The experimental data of Lambert [22] and Noyau [24] are reported for comparison.

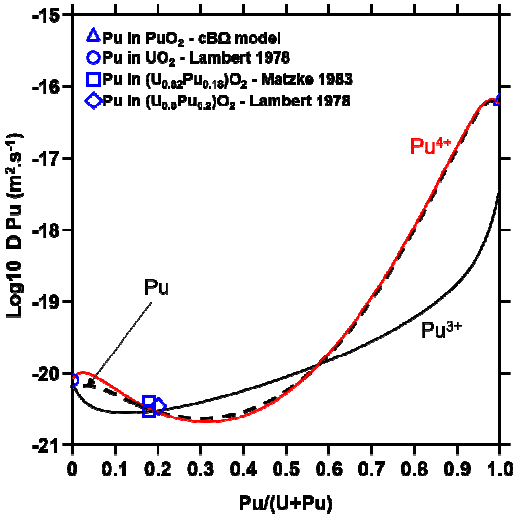

Figure 7: Calculated Pu diffusion coefficient against Pu/(U+Pu) ratio in $(U,Pu)O_2$ at 1773 K at the exact stoichiometry. Black dashed line represents the total Pu diffusion coefficient, while red and black lines are for Pu^{4+} and Pu^{3+}, respectively.

Compounds	E_{act}(eV) DICTRA	E_{act} (eV) exp. or calc.	D_0 ($m^2 \cdot s^{-1}$) DICTRA	D_0 ($m^2 \cdot s^{-1}$) exp. or calc.	Reference
PuO_2	4.0	4.0	$1.1\ 10^{-5}$	$1.2\ 10^{-5}$	cBΩ (our work)
UO_2	5.8	5.6	$1.9\ 10^{-4}$	$6.5\ 10^{-5}$	Lambert [22]
$(U_{0.85}Pu_{0.15})O_{2+x}$	5.5	3.8	$1.4\ 10^{-3}$	$2.5\ 10^{-6}$	Riemer [19]
$(U_{0.80}Pu_{0.20})O_{2\pm x}$	5.6 (O/M=1.9) 5.9 (O/M)=2 5.5 (O/M=2.1)	5.7 (I_{Pu})# 8.8 (S) # 3 (V_{Pu}) #	$2.5\ 10^{-4}$ $1.6\ 10^{-4}$ $1.9\ 10^{-3}$	-	Matzke [23]
$(U_{0.75}Pu_{0.25})O_2$	5.8	7.45-8.47* (V_{Pu}) 11.2 (I_U)	$7.8\ 10^{-5}$	-	Cheik Njifon [27]
$(U_{0.55}Pu_{0.45})O_{2-x}$	5.5	6.48	$1.7\ 10^{-5}$	$1.1\ 10^{-3}$	Noyau [24]

Table 5: Comparison of activation energy and prefactor data for Pu self-diffusion in PuO_2, UO_2 and $(U,Pu)O_{2\pm x}$. I_{Pu}, V_{Pu}, S denote Pu interstitial, Pu vacancy, Schottky defects, respectively. *: data calculated for neutral or charged (-4) Pu vacancy. #: data extracted from figure 13 in [23].

5. Conclusion

We have developed a mobility database for plutonium self-diffusion in $(U,Pu)O_{2\pm x}$ dioxide in connection with the thermodynamic model in [10,11] and the oxygen mobility database published in [9]. The mobility database was built using the DICTRA code, in which the mobility of Pu is described as a linear combination of the mobilities of Pu^{4+} and Pu^{3+}. The work was divided in two parts: (i) the creation/selection of relevant data of plutonium diffusion coefficients and (ii) the fitting of the mobilities Pu^{4+} and Pu^{3+}.

The first part – creation/selection of relevant data – is indeed the key of the present work. Unfortunately, the review of the experimental data reveals that very few data are available, and when they are available some of

460 them are inconsistent with each other. We chose here to use the so-called cBΩ model to produce more data for pure PuO_2. In addition, we reduced drastically the number of mobility parameters, based on physical arguments.

Then, the fitting of plutonium mobilities leads to an overall reliable description of plutonium diffusion in MOX as a function of temperature and oxygen stoichiometry, thanks to the change in the charge of the cations (Pu^{3+},Pu^{4+},U^{3+},U^{4+},U^{5+}) and oxygen defects (vacancy and interstitial).

465

Acknowledgments

This research is part of the INSPYRE project, which has received funding from the Euratom research and training program 2014-2018 under Grant Agreement No 754329. This research contributes to the joint program on nuclear materials (JPNM) of the European energy research alliance (EERA).

References

[1] D. Baron, L. Hallstadius, Fuel performance of light water reactors (uranium oxide and MOX), in: R. Konings, T. Allen, R. Stoller, S. Yamanaka (Eds.), Comprehensive Nuclear Materials (Vol-II), Elsevier, Amsterdam, 2012.

[2] J. E. Kelly, Generation IV international forum: A decade of progress through international cooperation, Progress Nucl. Ener. 77 (2014) 240.

[3] D. C. Crawford, D. L. Porter, S. L. Hayes, Fuels for sodium-cooled fast reactors: US perspective, J. Nucl. Mater. 371 (2007) 202.

[4] T. Markin, R. Street, The Uranium-Plutonium-Oxygen ternary phase diagram, J. Inorg. Nucl. Chem. 29 (1967) 2265.

[5] D. Staicu, Thermal properties of irradiated UO_2 and MOX, in: R. Konings, T. Allen, R. Stoller, S. Yamanaka (Eds.), Comprehensive Nuclear Materials (Vol-II), Elsevier, Amsterdam, 2012.

[6] M. Welland, Matter transport in fast reactor fuels, in: R. Konings, T. Allen, R. Stoller, S. Yamanaka (Eds.), Comprehensive Nuclear Materials (Vol-III), Elsevier, Amsterdam, 2012.

[7] T. Abe, K. Asakura, Uranium oxide and MOX production, in: R. Konings, T. Allen, R. Stoller, S. Yamanaka (Eds.), Comprehensive Nuclear Materials (Vol-II), Elsevier, Amsterdam, 2012.

[8] C. Guéneau, A. Chartier, L. Van Brutzel, Thermodynamic and Thermophysical Properties of the Actinide Oxides, in: R. Konings, T. Allen, R. Stoller, S. Yamanaka (Eds.), Comprehensive Nuclear Materials (Vol-II), Elsevier, Amsterdam, 2012.

[9] E. Moore, C. Guéneau, J.-P. Crocombette, Oxygen diffusion model of the mixed $(U,Pu)O_{2-x}$: Assessment and application, J. Nucl. Mater. 485 (2017) 216.

[10] C. Guéneau, N. Dupin, B. Sundman, C. Martial, J.-C. Dumas, S. Gossé, S. Chatain, F.D. De Bruycker, D. Manara, R.J.M. Konings, Thermodynamic modelling of advanced oxide and carbide nuclear fuels: Description of the U-Pu-O-C systems, J. Nucl. Mater. 419 (2011) 145.

[11] E. Moore, Thèse, Ecole Polytechnique (2013).

[12] E. Moore, C. Guéneau, J.-P. Crocombette, Diffusion model of the non-stoichiometric uranium dioxide, J. Sol. State Chem. 203 (2013) 145.

[13] P. Varotsos, K. Alexopoulos, Calculation of diffusion coefficients at any temperature and pressure from a single measurement. I. Self-diffusion, Phys. Rev. B22 (1980) 3130.

[14] P. Varotsos, K. Alexopoulos, Decisive importance of the bulk modulus and the anharmonicity in the calculation of migration and formation volumes, Phys. Rev. B24 (1981) 904.

[15] Thermo-Calc software, https://www.thermocalc.com/

[16] S. Hallström, L. Höglund, J. Ågren, Modelling of iron diffusion in the iron oxides magnetite and hematite with variable stoichiometry, Acta Mater. 59 (2011) 53.

[17] C. Matthews, R. Perriot, M. W.D. Cooper, C. R. Stanek, D. A. Andersson, Cluster dynamics simulation of uranium self-diffusion diffusion during irradiation in UO_2, J. Nucl. Mater. 527 (2019) 151787

[18] R. Lindner, D. Reimann and F. Schmitz, Plutonium as Reactor Fuel, IAEA, Vienna (1967) 265.

[19] G. Riemer and H.L. Scherff, Plutonium diffusion in hyper-stoichiometric mixed uranium-plutonium dioxides, J. Nucl. Mater. 39 (1971) 183.

[20] Hj. Matzke, Lattice disorder and metal self-diffusion in non-stoichiometric UO_2 and $(U,Pu)O_2$, J. Phys. Suppl. 11-12, 34 (1973) C9-317.

[21] F. Schmitz and A. Marajowsky, Thermodynamics of Nuclear Materials 1974, IAEA Vienna (1975) 467.

[22] R. A. Lambert, Thesis, University of Surrey (1978).

[23] Hj. Matzke, Diffusion processes and surface effects in non-stoichiometric nuclear fuel oxides UO_{2+x} and $(U,Pu)O_{2\pm x}$, J. Nucl. Mater. 114 (1983) 121.

[24] S. Noyau, Thèse, Université de Limoges (2012).

[25] T. Kutty, P. Hedge, K. Khan, S. Majumdar, D. Purushotham, Sintering studies on UO_2 – PuO_2 pellets with varying PuO_2 content using dilatometry, J. Nucl. Mater. 282 (2000) 54.

[26] L.-F. Wang, B. Sun, H.-F. Liu, D.-Y. Lin, H.-F. Song, Thermodynamics and kinetics of intrinsic point defects in plutonium dioxides, J. Nucl. Mater. 526 (2019) 151762.

[27] I. Cheik Njifon, Thèse, Université Aix-Marseille (2018).

[28] A.D. King, J. Moerman, Calcium diffusion in pure and YF_3-doped single crystal CaF_2, Phys. Stat. Sol. 22 (1974) 455.

[29] K. Compaan, Y. Haven, Correlation factors for diffusion in solids, Trans. Faraday Soc. 52 (1956) 786.

[30] E. Eser, H. Koc, M. Gokbulut, G. Gursoy, Estimations of heat capacities for actinide dioxide: UO_2, NpO_2, ThO_2, and PuO_2, Nucl. Eng. Tech. 46 (2014) 863.

[31] S. Hull, T.W.D. Farley, W. Hayles, M.T. Hutchings, The elastic properties of lithium oxide and their variation with temperature, J. Nucl. Mater. 160 (1988) 125.

[32] J.K. Fink, Thermophysical properties of uranium dioxide, J. Nucl. Mater. 279 (2000) 1.

[33] T. Yamashita, N. Nitani, T. Tsuji, H. Inagaki, Thermal expansions of NpO_2 and some other actinide dioxides, J. Nucl. Mater. 245 (1997) 72.

[34] M. Idiri, T. Le Bihan, S. Heathman, J. Rebizant, Behavior of actinide dioxides under pressure: UO_2 and ThO_2, Phys. Rev. 70 (2004) 14113.

[35] D.-J. Kim, Lattice parameters, ionic conductivities, and solubility limits in fluorite structure MO_2 oxide [M = Hf^{4+}, Zr^{4+}, Ce^{4+}, Th^{4+}, U^{4+}] solid solutions, J. Am. Ceram. Soc. 72 (1989) 1415.

[36] K. Ando, M. Akiyama, Y. Oishi, Lattice diffusion coefficient of oxygen in lithium oxide, J. Nucl. Mater. 95 (1980) 259.

[37] Hj Matzke, Atomic transport properties in UO_2 and mixed oxides $(U,Pu)O_2$, J. Chem. Soc., Faraday Trans. 2, 83 (1987) 1121.

[38] A.D. King, Thorium diffusion in single crystal ThO_2, J. Nucl. Mater. 38 (1971) 347.